

RESEARCH LETTER

10.1002/2015GL065854

Key Points:

- In most models extreme precipitation does not depend on emissions scenario

Supporting Information:

- Supporting Information S1

Correspondence to:

A. G. Pendergrass,
apgrass@ucar.edu

Citation:

Pendergrass, A. G., F. Lehner, B. M. Sanderson, and Y. Xu (2015), Does extreme precipitation intensity depend on the emissions scenario?, *Geophys. Res. Lett.*, 42, 8767–8774, doi:10.1002/2015GL065854.

Received 19 AUG 2015

Accepted 30 SEP 2015

Accepted article online 5 OCT 2015

Published online 29 OCT 2015

Does extreme precipitation intensity depend on the emissions scenario?

Angeline G. Pendergrass¹, Flavio Lehner¹, Benjamin M. Sanderson¹, and Yangyang Xu¹
¹National Center for Atmospheric Research, Boulder, Colorado, USA

Abstract The rate of increase of global-mean precipitation per degree global-mean surface temperature increase differs for greenhouse gas and aerosol forcings and across emissions scenarios with differing composition of change in forcing. We investigate whether or not the rate of change of extreme precipitation also varies across the four emissions scenarios that force the Coupled Model Intercomparison Project, version 5 multimodel ensemble. In most models, the rate of increase of maximum annual daily precipitation per degree global warming in the multimodel ensemble is statistically indistinguishable across the four scenarios, whether this extreme precipitation is calculated globally, over all land, or over extratropical land. These results indicate that in contrast to mean precipitation, extreme precipitation depends on the total amount of warming and does not depend on emissions scenario in most models.

1. Introduction

Extreme precipitation events cause flooding and impact society, infrastructure, and the land surface; therefore, it is important to understand how they might change in a warming climate. Observations show precipitation extremes have already increased with twentieth-century warming driven by anthropogenic forcing [Min *et al.*, 2011; Zhang *et al.*, 2013], and climate model projections show further increases throughout the twenty-first century [e.g., Pendergrass and Hartmann, 2014a].

Global-mean surface temperature change is closely tied to top-of-atmosphere (TOA) radiative forcing and is not particularly sensitive to the makeup of the forcing [Hansen *et al.*, 2005]. In contrast, the rate of increase of global-mean precipitation with warming does depend on the forcing agent. For example, it differs among forcing from greenhouse gas (GHG), reflecting aerosol [Andrews *et al.*, 2009], and absorbing aerosol [Ming *et al.*, 2010; Shiogama *et al.*, 2010; Frieler *et al.*, 2011; Pendergrass and Hartmann, 2012]. This is because the rate of precipitation change is tied to atmospheric radiative cooling when averaged globally over a long enough time period [Allen and Ingram, 2002; Pendergrass and Hartmann, 2014b] and atmospheric radiative cooling differs among forcing agents.

We have reason to expect that extreme precipitation will change differently from mean precipitation. Extreme precipitation events are driven by moisture convergence [Trenberth, 1999], and changes in their intensity are mostly driven by moistening of the atmosphere [Chou *et al.*, 2012]. Since changes in moisture closely follow changes in temperature (because changes in relative humidity with warming are small, [Held and Soden, 2006]) we anticipate that the change in intensity of extreme precipitation events would scale with the change in surface temperature, independent of the makeup of forcing agent.

Robust scaling of extreme precipitation with temperature across a wide range of forcing scenarios would be important for applications such as integrated assessment modeling, which does not simulate climate explicitly. Integrated assessment models contain simplified representations of climate in order to include more sophisticated infrastructure, economy, and ecosystem components [van Vuuren *et al.*, 2012].

In this paper, we test the hypothesis that extreme precipitation does not depend on emissions scenario, in contrast to mean precipitation, by analyzing climate model simulations with a range of emissions scenarios. In the next section, we describe the climate model simulations and our analysis. In the following section, we contrast the dependence of mean and extreme precipitation change across emissions scenario. The final section contains concluding remarks.

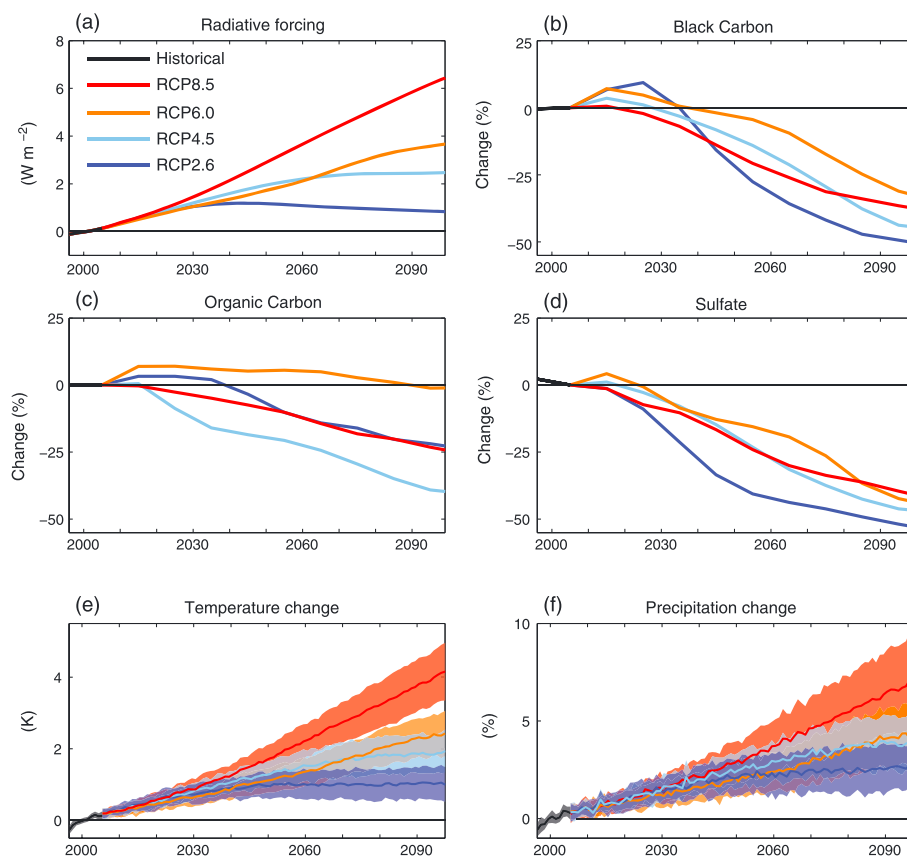


Figure 1. (a) TOA radiative forcing in the RCP scenarios and the historical period, relative to mean values from 1996 to 2005. Data are from *Meinshausen et al.* [2011]. Change in global-mean (b) black carbon, (c) organic carbon, and (d) sulfate emissions for the historical period and RCP scenarios, relative to mean values from 2000. Data from *Lamarque et al.* [2011]. Both hydrophilic and hydrophobic components of black carbon are included. (e) Global-mean surface air temperature anomalies relative to 1996–2005 and (f) global-mean precipitation relative to 1996–2005 values for each CMIP5 model simulation. Lines indicate the CMIP5 multimodel mean, and patches indicate ± 1 standard deviation.

2. Climate Model Simulations

The Coupled Model Intercomparison Project, version 5 (CMIP5) ensemble [Taylor et al., 2012] contains model simulations forced by four Representative Concentration Pathway (RCP) emissions scenarios [Mosset al., 2010], each starting from a corresponding historical simulation. The RCP scenarios are named for their approximate radiative forcings relative to the preindustrial period: 2.6, 4.5, 6.0, and 8.5 W m^{-2} at the end of the 21st century. This ensemble of simulations provides an opportunity to investigate whether or not changes in extreme precipitation depend on forcing agent.

Each emissions scenario specifies GHG concentrations and aerosol emissions. Most of the radiative forcing change in the RCP scenarios is driven by GHGs, which increase more in RCP8.5 than RCP2.6 (Figure 1a). The changes in aerosol forcing, on the other hand, are more similar across emissions scenarios. The black carbon emissions are shown in Figure 1b. They decrease by 50% over the 21st century. Organic carbon emissions (Figure 1c) also decrease in most scenarios, though their variation across RCP scenario is not monotonic. Sulfate emission changes (Figure 1d) closely follow black carbon emission changes. The differing fraction of the change in radiative forcing due to GHG and aerosol across the RCP scenarios provides variation against which to test our hypothesis.

For each model simulation in CMIP5, we calculate the changes in mean and extreme precipitation as the regression of annual precipitation data against global, annual mean surface temperature from the beginning of the scenario (2006) until the end of the 21st century (2100), with a decadal running average applied before regression. We quantify extreme precipitation as the maximum daily rainfall accumulation each year, which is the Rx1day extreme precipitation metric [Sillmann et al., 2013]. First, each model's daily accumulated

Table 1. CMIP5 Models Analyzed Here, Along With Their Changes in Extreme and Mean Precipitation in RCP8.5, Ordered From Highest to Lowest Increase in Extreme Precipitation in RCP8.5^a

	Model	$\Delta P / \Delta T$ (% K ⁻¹)	$\Delta R_{x1day} / \Delta T$ (% K ⁻¹)
1.	GFDL-ESM2M	0.9	11.3
2.	MRI-CGCM3	2.4	10.1
3.	GFDL-ESM2G	1.0	10.1
4.	IPSL-CM5A-MR	2.2	9.6
5.	IPSL-CM5A-LR	2.2	8.8
6.	CESM1-CAM5	1.6	8.3
7.	CCSM4	1.6	7.1
8.	BCC-CSM1-1-M	1.9	6.6
9.	GFDL-CM3	1.8	5.6
10.	BCC-CSM1-1	1.7	5.3
11.	NORES1-M	1.7	4.6
12.	MIROC5	1.1	4.5
13.	HADGEM2-AO	1.2	4.0
14.	CSIRO-MK3-6-0	2.0	4.0
15.	MIROC-ESM	1.7	2.4
16.	MIROC-ESM-CHEM	1.8	2.4
	CESM1-CAM5-LE	1.6	7.4

^aThe CESM Large Ensemble (LE) Mean is Included for Comparison.

precipitation is regridded (conserving total precipitation) onto a 2.5 by 2.5° grid. Then, the maximum for each year at each grid point is calculated. Next, the area-weighted global mean is taken. Finally, a decadal running average is applied. The change in extreme precipitation is the regression of this quantity onto global, decadal running mean surface air temperature over the 94 years of each scenario normalized by its mean over the years 1971–2000. It has units of % K⁻¹. Regressing the mean and extreme precipitation against each simulation's global-mean surface air temperature accounts for the influence of differing climate sensitivity among models and differing rates of warming across emissions scenarios. We use only one ensemble member (r1i1p1) from each of the CMIP5 models with sufficient archived data, listed in Table 1. We also performed the analysis using epoch differences between the last ten years of the historical simulations and the last ten years of the RCP scenarios and defining extreme precipitation as the 99.9th percentile precipitation rate (following Pendergrass and Hartmann [2014a]); our conclusions are robust to these variations in analysis method.

Global-mean surface air temperature (Figure 1e) and global-mean precipitation (Figure 1f) increase more for higher emissions scenarios, as expected from the range of radiative forcings driving them. For most of this paper, we will focus on quantities normalized by the change in global-mean surface temperature increase to test our hypothesis, but it is important to remember that there are drastically different amounts of absolute warming and also precipitation change across the scenarios, driven by the differences in forcing. Also, within each scenario the projected increases in temperature and precipitation vary across models (Figures 1e and 1f).

In addition to the differences across models, simulations from the same model with different initial conditions are subject to large internal variability [Deser *et al.*, 2012], especially for a noisy field like precipitation. In order to quantify the contribution of internal variability to the intermodel spread, we analyze an initial condition ensemble of the National Center for Atmospheric Research's Community Earth System Model, version 1.1 (CESM1.1), which we will refer to as the CESM single-model ensemble. Internal variability may differ among models, so the values from CESM shown here should be considered only an estimate of its magnitude. The CESM single-model ensemble consists of 30 members forced with the RCP8.5 scenario [Kay *et al.*, 2014], 14 members forced with the RCP8.5 scenario with aerosols held fixed at 2005 values, and 15 members forced with the RCP4.5 scenario (ending in 2080). We use all available years and simulations from the CESM single-model ensemble, despite that the RCP4.5 ensemble ends in 2080.

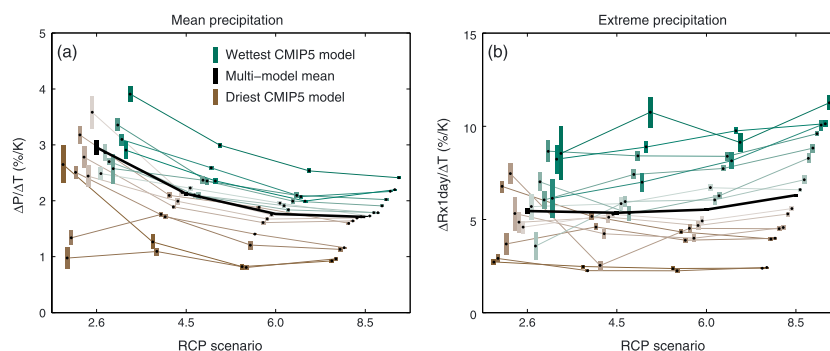


Figure 2. (a) Global-mean precipitation regressed against global-mean surface temperature change for the four RCP scenarios. Each colored bar represents one CMIP5 simulation; the color of the bar and its offset from the scenario indicate the model's rank in RCP8.5. Black bars show the regression of the CMIP5 multimodel mean. Bar length indicates the 95% confidence interval of each regression coefficient. (b) As in Figure 2a but for the regression of globally-averaged maximum annual 1 day rainfall against global-mean surface air temperature. Note the different y axes.

3. Mean and Extreme Precipitation Change Across the Emissions Scenarios

In this section, we will contrast the changes in mean and extreme precipitation with warming across the RCP scenarios. The change in global-mean precipitation per degree global-mean surface air temperature change for each model and RCP scenario is shown in Figure 2a, along with its 95% confidence intervals (which are calculated following *Draper and Smith* [1981] using Matlab R2012a's regress function). The value for each model in RCP8.5 is listed in Table 1. To test for differences in the rate of change of precipitation with emissions scenario, in the multimodel mean we compare the 84% confidence intervals between scenarios [*Payton et al.*, 2003]. To test for differences across scenarios within individual models, we tabulate whether the change in precipitation is smaller or larger between adjacent scenario pairs for each model, then sum over all models and scenario pairs and evaluate statistical significance with the Signs test (see Text S1 and Figure S1 in the supporting information for details). The rate of change of mean precipitation per degree warming decreases systematically with increasing emissions scenario in the multimodel mean; for individual models differences are also significant.

We can understand the decrease in mean precipitation with increasing emissions scenario as follows. Precipitation-induced latent heat release must be balanced by atmospheric radiative cooling and sensible heat flux, a fundamental constraint governing its change [e.g., *Pendergrass and Hartmann*, 2014b]. The change in atmospheric radiative cooling, and thus global-mean precipitation, per degree warming for any component of the forcing in isolation (GHG or aerosols) is similar across emissions scenarios. Surface warming leads to increased atmospheric radiative cooling and thus increased precipitation. On the other hand, the direct radiative effect of increased GHGs leads to *decreased* atmospheric radiative cooling and decreased precipitation. Accounting for the direct radiative effect of GHGs as well as the associated warming, their net effect is an increase in atmospheric radiative cooling and precipitation, at a smaller rate of increase ($1.2\text{--}1.3\text{ W m}^{-2}\text{ K}^{-1}$) than for warming alone ($2.4\text{--}2.8\text{ W m}^{-2}\text{ K}^{-1}$) [*Pendergrass and Hartmann*, 2014b]. Another factor driving the increase in precipitation in the RCP scenarios is the change in aerosol forcing. Decreasing absorbing aerosol forcing (primarily black carbon) over the 21st century leads directly to a decrease in shortwave absorption and thus an increase in precipitation [*Pendergrass and Hartmann*, 2012]. Decreasing sulfate and organic carbon aerosols do not change atmospheric radiative cooling directly, but they do induce warming that drives increasing precipitation. The higher emissions scenarios have larger increases in GHG forcing, but all four emissions scenarios have a similar magnitude decrease in absorbing aerosol forcing. Therefore, in the higher emissions scenarios the increase in precipitation due to decreasing absorbing aerosol forcing makes up a smaller fraction of the total increase in precipitation. Overall, atmospheric radiative cooling and precipitation increase less in higher emissions scenarios (see Figure 2a).

The CESM single-model ensemble excludes structural (or parametric) uncertainty, so variations across CESM ensemble members is due to internal variability alone. The spread in global-mean precipitation per degree warming across members of the single-model ensemble (standard deviation of 0.038 \% K^{-1} for RCP8.5, not shown) is much smaller than the spread across the CMIP5 multimodel ensemble (0.44 \% K^{-1} in RCP8.5, Figure 2a). This indicates that most of the difference in mean precipitation increase across CMIP5 models is

due to structural differences among models, rather than internal variability. In the CESM ensemble, the change in global-mean precipitation per degree warming is larger in RCP4.5 than RCP8.5 in all ensemble members, consistent with the CMIP5 multimodel ensemble. The RCP8.5 ensembles with changing and fixed aerosols allow us to isolate the effect of aerosol forcing. With fixed aerosol forcing, the rate of increase of global-mean precipitation is $0.3\% \text{ K}^{-1}$ smaller than in RCP8.5 with decreasing aerosol forcing, consistent with the decreasing aerosol forcing, which is in all of the RCP scenarios, leading to increased precipitation.

We have seen that the change in mean precipitation per degree warming depends on emissions scenario. Is this also the case for the change in extreme precipitation? We expect that it might not be because extreme precipitation depends mostly on moisture convergence and changes in circulation with warming in climate model projections are small [Trenberth, 1999]. Figure 2b shows the multimodel mean change in extreme precipitation (the change in annual maximum daily rainfall rate per degree warming) for each RCP scenario; the change in extreme precipitation in RCP8.5 for each model is listed in Table 1. The multimodel mean change in extreme precipitation in RCP8.5 is $6.3\% \text{ K}^{-1}$. The changes in multimodel mean extreme precipitation in RCP2.6, 4.5, and 6.0 are statistically indistinguishable, indicated by the overlap in 84% confidence intervals, while the change for RCP8.5 is slightly larger. There is a large range of extreme precipitation change with warming across the CMIP5 models, which has been shown in previous studies [e.g., O'Gorman, 2012; Kharin et al., 2013]. Nonetheless, extreme precipitation does not have significantly different changes across scenarios according to the Signs test (Figure S1 and Text S1).

Kharin et al. [2013] also examine the changes in mean and extreme precipitation, using a slightly different definition of extreme precipitation and performing epoch differences; their results (particularly Figure 5) appear consistent with the idea that the rate of extreme precipitation change largely does not vary across emissions scenario, while mean precipitation change does. Peacock [2012] shows that extreme precipitation does not vary across the RCP emissions scenarios in integrations of CCSM4 with one ensemble member per RCP scenario.

The portion of the intermodel spread in global extreme precipitation increase attributable to internal variability in the CESM large ensemble is still small compared to the total intermodel spread, accounting for $0.17\% \text{ K}^{-1}$ (not shown), while the spread of response across CMIP5 models in RCP8.5 is $2.9\% \text{ K}^{-1}$ (Figure 2b).

Four of the CMIP5 models have an increase in extreme precipitation with emissions scenario; these models also have relatively large increases in extreme precipitation in RCP8.5 (Table 1 and Figure S1b, models 2, 3, 5, and 7). Generally, the CMIP5 model simulations have a large range in global extreme precipitation response. Pendergrass and Hartmann [2014a] also found a large range in the extreme precipitation response at the heaviest rain rates. They defined an “extreme mode” response as a large increase in the rain rate for the heaviest events and found that it scales with the magnitude of warming and is concentrated in the tropics. We speculate that the models with an increase in extreme precipitation with emissions scenario have an extreme mode response.

We can further explore the spatial distribution of the response of extreme precipitation to warming. Figure 3a shows a map of the CMIP5 multimodel mean change in extreme precipitation defined locally per degree global-mean surface temperature increase. Figure 6a of Kharin et al. [2013] is similar, though normalized by local surface temperature change. Patterns in the tropics are similar in both cases, but at high latitudes the change in extreme precipitation is smaller when normalized by local surface temperature change due to polar amplification. The extreme precipitation change with warming is surprisingly uniform and positive over most of the globe (Figure 3a), in contrast to mean precipitation change (Figure 3c). It has peaks over the equatorial Pacific, Africa, the Arabian Peninsula and India, and minima in the subtropical eastern ocean basins and the Mediterranean. These minima extend below zero, indicating decreases in extreme precipitation with warming (consistent with Fischer et al. [2014]).

Figure 3b shows the ratio of the CMIP5 multimodel mean change in extreme precipitation to the standard deviation across the models, as a measure of the signal to noise at each location. While the change in extreme precipitation is large in some regions in the tropics, the signal relative to the intermodel spread is largest in the extratropics. This is especially clear in the zonal mean and is in stark contrast to the case for seasonal warming, where the emergence of a signal occurs in the tropics first [Diffenbaugh and Scherer, 2011]. The signal-to-noise pattern for extreme precipitation change largely follows that of mean precipitation change

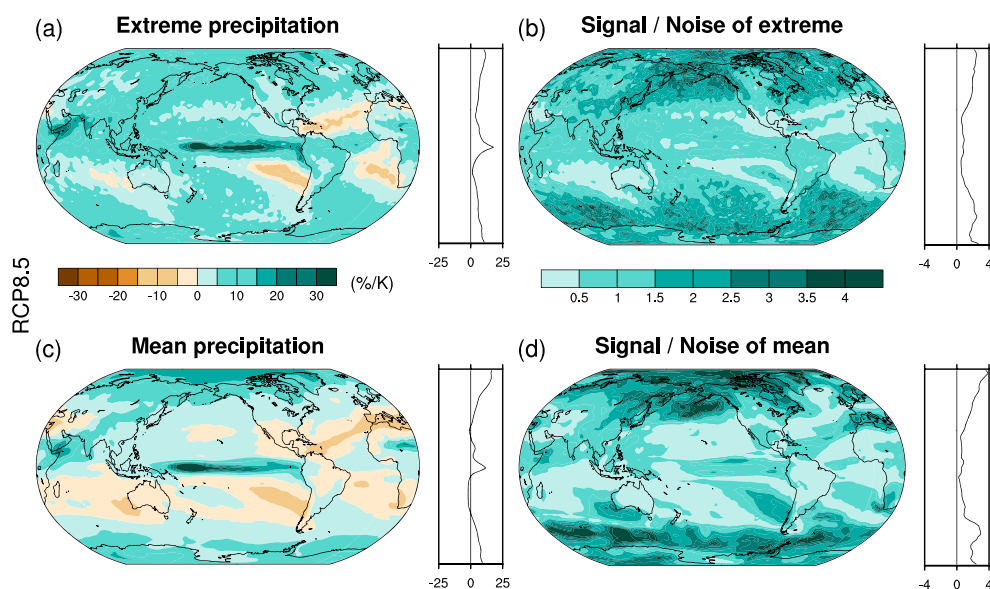


Figure 3. (a) The CMIP5 multimodel mean change in extreme precipitation regressed against global-mean surface temperature change in the RCP8.5 scenario and (b) the ratio of the absolute value of the multimodel mean extreme precipitation change to its standard deviation across models, as a measure of signal to noise. (c and d) As in Figures 3a and 3b for mean precipitation. Shown to the right of each map is its zonal mean. Note the differing color scales and units among the panels.

(Figure 3d), though for extreme precipitation change the ratio is larger in most of the tropics and smaller in the extratropics.

Many impacts of extreme precipitation, for example, flooding, only occur over land. For applications that examine the impacts of extreme precipitation, such as pattern scaling [Tebaldi and Arblaster, 2014], the change in extreme precipitation over land is more important than the change over ocean. Since most of the heaviest precipitation events on the globe occur over the ocean in the tropics, we might expect our results to differ between the tropics and extratropics and over land and ocean.

Figure 4a shows the change in extreme precipitation over land per degree global-mean surface temperature increase. We normalize by global-mean surface temperature change for consistency with Figure 2b, though the change in surface temperature over land would be slightly larger and noisier than the change in global-mean surface temperature. There are two models with much larger increases in extreme precipitation than the others in RCP8.5, but changes across scenarios are not significantly different according to the Signs test (which aggregates across all models).

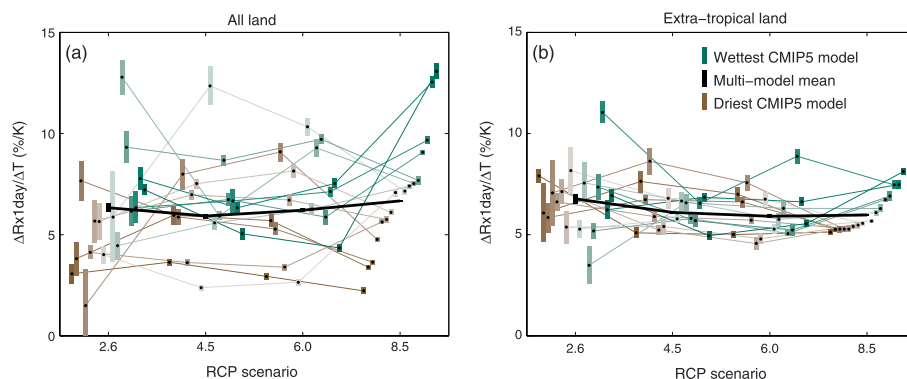


Figure 4. (a) The change in maximum annual daily rainfall over all land regressed against global-mean surface temperature change for the four RCP scenarios. Symbols as in Figure 2. (b) As in Figure 4a for the change in maximum annual daily rainfall over extratropical land regressed against global-mean surface temperature change.

Finally, we might expect that the response of extreme precipitation in the tropics and extratropics would behave differently, since precipitating systems at these latitudes are governed by different dynamics. Figure 4b shows the rate of change of extreme precipitation over land in the extratropics (which we define as poleward of 30° in both hemispheres). The multimodel mean change decreases slightly with increasing scenario, while the differences across scenario for individual models are not statistically different according to the Signs test. The range of responses decreases with increasing emissions scenario, reflecting an increase in signal relative to noise with larger warming. The intermodel spread is smaller when we restrict the analysis to extratropical land than for all land (Figure 4b), consistent with the larger signal-to-noise ratio in the extratropics. For the CESM single-model ensemble, extreme precipitation change (not shown) is also very similar across the scenarios.

In RCP8.5, the spread across the CESM single-model ensemble ($0.17\% \text{ K}^{-1}$) is about 20% of that across the CMIP5 multimodel ensemble ($0.97\% \text{ K}^{-1}$), indicating that internal variability constitutes an increased fraction of the intermodel spread in extratropical land extreme precipitation change across the CMIP5 models. When using the alternative method of the difference between 10 year epochs at the beginning and end of the century, the internal variability constitutes nearly half of the spread across the CMIP5 multimodel ensemble. This reflects mainly the smaller magnitude of structural differences across models in the extratropics compared with the tropics. Models agree better on the response of extreme precipitation in the extratropics than globally (compare Figures 4b and 2b), which we speculate is because in the extratropics most precipitating systems have larger spatial scales and are driven by dynamics that are comparatively well represented in climate models. Whereas structural uncertainty in projections of extreme precipitation change can be reduced, uncertainty due to internal variability is irreducible [Deser *et al.*, 2012]. In this sense, there is a larger opportunity to improve projections of extreme precipitation change in the tropics than over land in the extratropics.

4. Conclusions

We have examined the rate of increase of extreme precipitation compared with global-mean precipitation across emissions scenarios in two ensembles of climate model simulations. We defined extreme precipitation as the maximum annual daily precipitation accumulation each year and examined its changes globally, over all land, and over extratropical land. The emissions scenarios which force the simulations have different changes in greenhouse gas forcing but similar changes in aerosol forcing. We find that in most models, the rate of extreme precipitation increase per degree warming does not depend on the emissions scenario, in contrast to mean precipitation. This means that the increase of extreme precipitation depends only on the magnitude of warming in these models and not on the composition of the change in forcing.

Moving to smaller spatial scales, from global to land and then extratropical land, the lack of dependence on scenario continues to be valid. Internal variability becomes an increasingly important contributor to the uncertainty of the change in extreme precipitation with warming, constituting about 20% of the intermodel spread in extreme precipitation change over extratropical land. In the tropics, there are large differences across models due to structural uncertainty. Some models have larger rates of increase of extreme precipitation for emissions scenarios with more total warming.

While we are relatively confident in our understanding of why mean precipitation changes at the rate that it does, we do not fully understand the structural differences across models that drive the large range of extreme precipitation response. Future work will explore the large changes in extreme precipitation present in some models: how it arises and whether or not it is realistic. While extreme precipitation change might be more straightforwardly related to warming than mean precipitation, there is still room to improve our understanding of how extreme precipitation changes with warming.

References

- Allen, M. R., and W. J. Ingram (2002), Constraints on future changes in climate and the hydrologic cycle, *Nature*, 419(6903), 224–232, doi:10.1038/nature01092.
- Andrews, T., P. M. Forster, and J. M. Gregory (2009), A surface energy perspective on climate change, *J. Clim.*, 22(10), 2557–2570, doi:10.1175/2008JCLI2759.1.
- Chou, C., C.-A. Chen, P.-H. Tan, and K. T. Chen (2012), Mechanisms for global warming impacts on precipitation frequency and intensity, *J. Clim.*, 25(9), 3291–3306, doi:10.1175/JCLI-D-11-00239.1.
- Deser, C., A. Phillips, V. Bourdette, and H. Teng (2012), Uncertainty in climate change projections: The role of internal variability, *Clim. Dyn.*, 38, 527–546, doi:10.1007/s00382-010-0977-x.

Acknowledgments

CMIP5 data are available from the PCMDI archive; thanks to the modeling groups for generating it and to PCMDI for administering it. CESM large ensemble integrations are available from NCAR at <https://www2.cesm.ucar.edu/models/experiments/LENS>. A.G.P. was supported by an NCAR Advanced Studies Program Postdoctoral research fellowship. Thanks to the NCAR/IMAGE Pattern Scaling Workshop for motivating the work (the workshop report is available online at <https://www2.image.ucar.edu/event/PS2014>). Joeri Rogelj provided insight about the RCP scenario forcings. We thank Claudia Tebaldi, Clara Deser, and two anonymous reviewers for their helpful feedback. The National Center for Atmospheric Research is sponsored by the National Science Foundation.

- Diffenbaugh, N. S., and M. Scherer (2011), Observational and model evidence of global emergence of permanent, unprecedented heat in the 20th and 21st centuries, *Clim. Change*, 107(3–4), 615–624, doi:10.1007/s10584-011-0112-y.
- Draper, N. R., and H. Smith (1981), *Applied Regression Analysis*, in *Wiley Series in Probability and Mathematical Statistics*, 2nd ed., 709 pp., John Wiley, New York.
- Fischer, E., J. Sedláček, E. Hawkins, and R. Knutti (2014), Models agree on forced response pattern of precipitation and temperature extremes, *Geophys. Res. Lett.*, 41, 8554–8562, doi:10.1002/2014GL062018.
- Frieler, K., M. Meinshausen, T. S. v. Deimling, T. Andrews, and P. Forster (2011), Changes in global-mean precipitation in response to warming, greenhouse gas forcing and black carbon, *Geophys. Res. Lett.*, 38, L04702, doi:10.1029/2010GL045953.
- Hansen, J., et al. (2005), Efficacy of climate forcings, *J. Geophys. Res.*, 110, D18104, doi:10.1029/2005JD005776.
- Held, I. M., and B. J. Soden (2006), Robust responses of the hydrological cycle to global warming, *J. Clim.*, 19(21), 5686–5699, doi:10.1175/JCLI3990.1.
- Kay, J. E., et al. (2014), The Community Earth System Model (CESM) large ensemble project: A community resource for studying climate change in the presence of internal climate variability, *Bull. Am. Meteorol. Soc.*, 96, 1333–1349, doi:10.1175/BAMS-D-13-00255.1.
- Kharin, V. V., F. W. Zwiers, X. Zhang, and M. Wehner (2013), Changes in temperature and precipitation extremes in the CMIP5 ensemble, *Clim. Change*, 119(2), 345–357.
- Lamarque, J.-F., G. P. Kyle, M. Meinshausen, K. Riahi, S. J. Smith, D. P. van Vuuren, A. J. Conley, and F. Vitt (2011), Global and regional evolution of short-lived radiatively-active gases and aerosols in the Representative Concentration Pathways, *Clim. Change*, 109(1–2), 191–212, doi:10.1007/s10584-011-0155-0.
- Meinshausen, M., et al. (2011), The RCP greenhouse gas concentrations and their extensions from 1765 to 2300, *Clim. Change*, 109(1–2), 213–241, doi:10.1007/s10584-011-0156-z.
- Min, S.-K., X. Zhang, F. W. Zwiers, and G. C. Hegerl (2011), Human contribution to more-intense precipitation extremes, *Nature*, 470(7334), 378–381, doi:10.1038/nature09763.
- Ming, Y., V. Ramaswamy, and G. Persad (2010), *Geophys. Res. Lett.*, 37, L13701, doi:10.1029/2010GL042895.
- Moss, R. H., et al. (2010), The next generation of scenarios for climate change research and assessment, *Nature*, 463(7282), 747–756.
- O’Gorman, P. A. (2012), Sensitivity of tropical precipitation extremes to climate change, *Nat. Geosci.*, 5(10), 697–700, doi:10.1038/NGEO1568.
- Payton, M. E., M. H. Greenstone, and N. Schenker (2003), Overlapping confidence intervals or standard error intervals: What do they mean in terms of statistical significance?, *J. Insect Sci.*, 3(1), 34 pp., doi:10.1093/jis/3.1.34.
- Peacock, S. (2012), Projected twenty-first-century changes in temperature, precipitation, and snow cover over North America in CCSM4, *J. Clim.*, 25(13), 4405–4429, doi:10.1175/JCLI-D-11-00214.1.
- Pendergrass, A., and D. Hartmann (2014a), Changes in the distribution of rain frequency and intensity in response to global warming, *J. Clim.*, 27(22), 8372–8383, doi:10.1175/JCLI-D-14-00183.1.
- Pendergrass, A., and D. Hartmann (2014b), The atmospheric energy constraint on global-mean precipitation change, *J. Clim.*, 27(2), 757–768, doi:10.1175/JCLI-D-13-00163.1.
- Pendergrass, A. G., and D. L. Hartmann (2012), Global-mean precipitation and black carbon in AR4 simulations, *Geophys. Res. Lett.*, 39, L01703, doi:10.1029/2011GL050067.
- Shiogama, H., et al. (2010), Emission scenario dependencies in climate change assessments of the hydrological cycle, *Clim. Change*, 99(1), 321–329, doi:10.1007/s10584-009-9765-1.
- Sillmann, J., V. Kharin, X. Zhang, F. Zwiers, and D. Bronaugh (2013), Climate extremes indices in the CMIP5 multimodel ensemble: Part 1. Model evaluation in the present climate, *J. Geophys. Res. Atmos.*, 118(4), 1716–1733, doi:10.1002/jgrd.50203.
- Taylor, K. E., R. J. Stouffer, and G. A. Meehl (2012), An overview of CMIP5 and the experiment design, *Bull. Am. Meteorol. Soc.*, 93(4), 485–498, doi:10.1175/BAMS-D-11-00094.1.
- Tebaldi, C., and J. M. Arblaster (2014), Pattern scaling: Its strengths and limitations, and an update on the latest model simulations, *Clim. Change*, 122(3), 459–471.
- Trenberth, K. E. (1999), Conceptual framework for changes of extremes of the hydrological cycle with climate change, in *Weather and Climate Extremes*, edited by T. R. Karl, N. Nicholls, A. Ghazi, pp. 327–339, Springer, Netherlands, doi:10.1007/978-94-015-9265-9_18.
- van Vuuren, D. P., L. B. Bayer, C. Chuwah, L. Ganzeveld, W. Hazeleger, B. van den Hurk, T. van Noije, B. O'Neill, and B. J. Strengers (2012), A comprehensive view on climate change: Coupling of earth system and integrated assessment models, *Environ. Res. Lett.*, 7(2), 024012, doi:10.1088/1748-9326/7/2/024012.
- Zhang, X., H. Wan, F. W. Zwiers, G. C. Hegerl, and S.-K. Min (2013), Attributing intensification of precipitation extremes to human influence, *Geophys. Res. Lett.*, 40(19), 5252–5257, doi:10.1002/grl.51010.